NOTE *Surgery*

Computed tomography and magnetic resonance imaging of thoracic chordoma in a Bengal tiger (*Panthera tigris tigris*)

Toshie ISERI[1)]*, Junichiro SHIMIZU[2)], Hideo AKIYOSHI[3)], Kayo KUSUDA[4)], Akiyoshi HAYASHI[3)], Keiichiro MIE[3)], Takeshi IZAWA[3)], Mitsuru KUWAMURA[3)], Jyoji YAMATE[3)], Yuka FUJIMOTO[3)] and Fumihito OHASHI[3)]

[1)]*Department of Veterinary Science, Joint Faculty of Veterinary Medicine, Yamaguchi University, 1677–1 Yoshida, Yamaguchi 753–8515, Japan*
[2)]*Uni Animal Hospital, 32–5 W17N1, Obihiro, Hokkaido 080–0047, Japan*
[3)]*Graduate School of Life and Environmental Sciences, Department of Veterinary Sciences, Osaka Prefecture University, 1–58 Rinku-oraikita, Izumisano, Osaka 598–8531, Japan*
[4)]*Misaki Park Zoo, 3990 Tannowa, Misaki-cho, Osaka 599–0301, Japan*

(Received 30 December 2014/Accepted 19 February 2015/Published online in J-STAGE 3 March 2015)

ABSTRACT. A Bengal tiger was presented for evaluation of weakness, ataxia and inappetance. Computed tomography (CT) and magnetic resonance imaging (MRI) revealed a mass extending from the T7-8 vertebral body to the left rib and compressing the spinal cord. On CT, the bone destruction and sequestrum were shown. On MRI, the multilobulated mass appeared hypo- to isointense in T1-weighted and hyperintense in T2-weighted images. The tiger died after imaging, most likely from renal failure. Chordoma without metastasis was diagnosed on necropsy. The imaging characteristics were similar to those found in chordoma in humans. This report describes the use of CT and MRI in an exotic species.

KEY WORDS: chordoma, computed tomography, magnetic resonance imaging, tiger

doi: 10.1292/jvms.14-0694; *J. Vet. Med. Sci.* 77(7): 857–860, 2015

Chordoma is rare malignant tumor of notochordal origin that may occur at any site along the embryonic notochord. A few cases of chordoma have been reported in dogs [5, 9, 10, 14, 18], a cat [1], rats [13] and minks [6]; in ferrets, several cases of tail chordoma have been reported [3]. Computed tomography (CT) and magnetic resonance imaging (MRI) are valuable for identifying chordomas in humans [19]. However, in the veterinary literature, the use of CT or MRI to characterize chordoma has been described in only a few case reports involving dogs [5, 10, 14, 18], and in none of these cases were both imaging modalities used for the same patient. This report is the first to describe CT and MRI characteristics of a chordoma in a Bengal tiger.

A 19-year-old female Bengal tiger (*Panthera tigris tigris*), weighing 100 kg, was presented for evaluation of a 2-month history of hindlimb weakness, ataxia and inappetance. Treatment with antibiotics, prednisolone and vitamin B complex did not alleviate these symptoms, and the tiger was referred to the Osaka Prefecture University for diagnostics and treatment included surgery.

The tiger was premedicated with an intramuscular injection of medetomidine, midazolam and butorphanol. General anesthesia was induced with an intramuscular injection of ketamine and maintained with isoflurane in oxygen, administered through a semi-closed anesthetic circuit via endotracheal intubation. Fluids (Ringer's acetate solution, 10 m*l*/kg/hr throughout the imaging examination) and contrast medium were delivered intravenously through a catheter placed in the cephalic vein.

CT from the head to the pelvic region, including the thorax and abdomen, was performed using a 16-slice multidetector computed tomography unit (Activion16, Toshiba Medical, Saitama, Japan). The tiger was imaged in ventral recumbency. The CT scanning parameters were as follows: 0.75 sec tube rotation time at 120 kVp and 200 mAs; slice thickness, 4 mm; helical pitch, 15.0; imaging field of view, 500 mm. Contrast-enhanced CT images were obtained 20 sec after contrast medium (iohexol 300 mgI/m*l*, Omnipaque® 300, 100 m*l*, Daiichi-Sankyo Co., Tokyo, Japan) was injected intravenously at a rate of 5 m*l*/sec using an auto-injector (Auto-Enhance A-60, Nemoto Kyorindo Co., Ltd., Tokyo, Japan). The reconstruction algorithms applied were bone and standard, with an image reconstruction interval of 2.0 mm. Window width (WW) and window level (WL) were adjusted slightly as needed for evaluation. Values were as follows: bone, WW=1,500 and WL=300; lung, WW=1,400 and WL= −500; abdomen, WW=350 and WL=40; spinal cord, WW=200 and WL=30.

After CT scanning was complete, MRI examination was performed using an 0.4-Tesla MRI system (APERTO Inspire, Hitachi, Tokyo, Japan). The imaging parameters were as follows: section thickness, 6.5 mm axial, 3.5 mm coronal; matrix size, 256 × 256; T1-weighted fast spin echo sequence (TR range/TE range), 300 msec/15 msec; T2-weighted fast spin echo sequence (TR range/TE range), 3,000 msec/120 msec with axial and coronal imaging at the

*CORRESPONDENCE TO: ISERI, T., Department of Veterinary Science, Joint Faculty of Veterinary Medicine, Yamaguchi University, 1677–1 Yoshida, Yamaguchi 753–8515, Japan.
e-mail: iseri@yamaguchi-u.ac.jp

thoracic vertebrae. Contrast-enhanced MRI was obtained using a T1-weighted fast spin echo after intravenous injection of 0.2 m//kg of gadopentetate dimeglumine (Magnevist, Bayer Health Care, Tokyo, Japan).

Routine monitoring during anesthesia for CT imaging showed no abnormal vital signs of this tiger. During the MRI, the magnetic equipment limited monitoring of anesthesia to manual assessments of pulse and mucus membrane color. Toward the end of the MRI examination, the quality of the pulse gradually decreased, and upon completion of MRI, the pulse could not be detected. We removed the tiger from the MRI gantry; an electrocardiogram showed that the patient had developed ventricular fibrillation. We began cardiopulmonary resuscitation using chest compressions, medication with atipamezole and epinephrine, and external defibrillation, but the tiger died. A postmortem examination was performed, as well as analyses of urine obtained at almost the same time of starting fluid therapy and of blood obtained immediately after death.

A mass was identified extending from the T7–8 vertebral bodies to the T7 left rib, with a maximum measured diameter of 6.0 × 5.7 × 3.0 cm. On CT imaging, the mass was largely hypodense (with a standard algorithm; data not shown), with bone destruction and erosion at the T7 vertebral body, and especially, bone sequestrum was represented (Fig. 1). Imaging obtained after the injection of contrast medium was not diagnostically useful, because the maximum volume possible with the auto-injector (100 m*l*) was insufficient for the size of the patient in this protocol. Metastatic lesions were not seen on CT images. On MR images, the mass was hypo- to isointense on T1 weighted images (Fig. 2A) and hyperintense on T2-weighted images (Fig. 2B). And, multiloblation was evident on the T2-weighted images. The mass showed enhancement on MR images obtained after injection of contrast medium (Fig. 2C). The mass involved the nerve sheath at T7-8 and compressed the spinal cord (Fig. 2D). Urinalysis revealed a high protein/creatinine ratio (163/98.9 mg/d*l*, or 1.65) and a low specific gravity (1.023). Serum analysis revealed that both blood urea nitrogen (123 mg/d*l*; baseline 23.4 ± 0.7 mg/d*l*) and serum creatinine (5.47 mg/d*l*; baseline 2.5 ± 0.1 mg/d*l*) were elevated, compared with values previously reported in the Bengal tiger [11]. Upon postmortem examination, swollen axons were found in the spinal cord at T7–8. The pathological diagnosis by immunohistochemical analysis was chordoma arising from the thoracic vertebrae (Fig. 3). Metastases were not observed. Necropsy also revealed moderate chronic nephropathy.

In humans, chordoma generally arises between the ages of 30 and 60 years [12] and are located in the axial skeleton, typically in the spheno-occipital region of the skull and the sacrum [19]. This tiger was geriatric at 19 years of age (the average life span of Bengal tigers is 15 years in the wild and 16–18 years in the zoo), but the tumor was located in the thoracic vertebrae and left rib, which is similar to the location in humans.

CT shows bony detail well, and osteolytic areas are commonly seen in cases of chordoma in humans [12]. A report of chordoma in a dog described areas of high attenuation

Fig. 1. Transverse CT imaging at T7, showing bone sequestrum with bone destruction and erosion.

resembling calcification within a cervical extradural mass [14]. However, intratumoral calcifications appear irregular at CT and are usually thought to represent sequestra from bone destruction rather than dystrophic calcifications in the tumor itself [4]; the CT finding was similar for this tiger. Previous studies of chordoma in human have reported that the MR signal of T1-weighted images was predominately hypointense or isointense [8, 19], with no tumors reported as hyperintense [17], and T2-weighted images of chordoma have been predominately hyperintense [8, 19] or isointense [17]. In a previous report in a dog, a chordoma also appeared hyperintense on a T2-weighted image [5]. Also, the common features of chordomas are multilobulated tumors [15]. In this tiger, T1-weighted images were hypo- to isointense and T2-weighted images were hyperintense, and multiloblation was evident on the T2-weighted images; these MRI findings are similar to those previously reported in humans and dogs. Furthermore, MRI showed that the chordoma involved the T7–8 spinal nerve sheath and compressed the spinal cord. In this patient, the clinical symptoms were consistent with the imaging diagnosis. It was thought that the compression of the T7-8 spinal cord caused hindlimb weakness and ataxia and that pain due to compression of the spinal cord caused the decrease in appetite. Because it is difficult to evaluate bone using MRI, combined CT and MRI imaging provides a better technique for the diagnosis and pretreatment evaluation of chordoma than does MRI alone [19].

According to previously published reports, chordoma in dogs has not been associated with metastases [9, 14], although local recurrence has been reported 25 months after surgical treatment [14]. Metastasis to a lymph node and the liver has been reported in one cat 10 months after surgical removal, without local recurrence [1]. The incidence of metastasis in humans has been reported to be 24.7%, with an

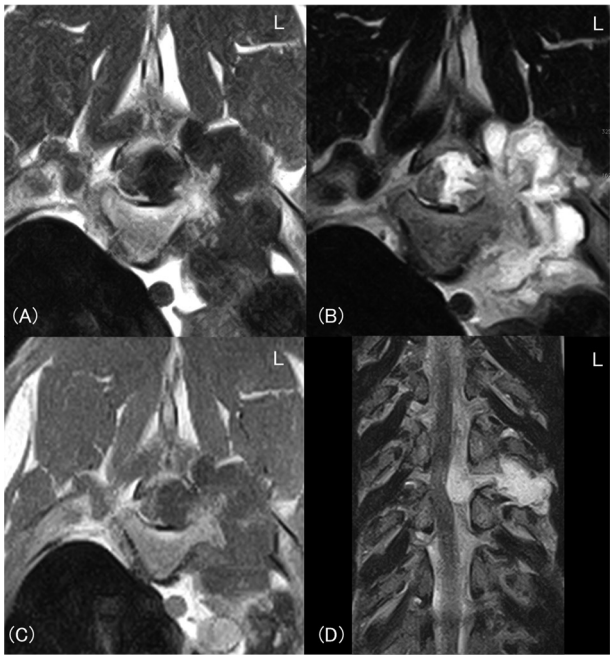

Fig. 2. (A) Transverse T1-weighted MRI at T7, showing a hypo- to isointense mass. (B) Transverse T2-weighted MRI at T7, showing a hyperintense mass, and multiloblation was evident. (C) Transverse T1-weighted MRI at T7 after injection of contrast medium, showing mass enhancement. (D) Coronal T2-weighted MRI at the thoracic spine, showing a mass involving the T7-8 spinal nerve sheath and compressing the spinal cord.

average of 45.0 months (range, 0–600 months) after initial diagnosis, and the common sites include the lung, lymph nodes, skin, liver and bone [8]. Metastases were not found in this tiger, either by CT imaging of the body or on necropsy. It was thought that the timing of CT and MRI examination was only 2 months after symptoms were first shown. The progress of treatment of chordoma, such as radiotherapy, in veterinary species will bring result in longer survival times, and therefore, the identification of metastases will become more important [12]. CT and MRI studies will be useful in diagnosing distant metastases of chordoma, which will directly affect the treatment plan.

Immediately after completion of the MRI, the tiger experienced cardiac arrest. Cardiopulmonary resuscitation was begun, but the tiger died. Blood biochemical examination immediately after death revealed elevated BUN (123 mg/d*l*) and creatinine (5.47 mg/d*l*). In humans, forensic pathologists often hesitate to use biochemical markers from blood obtained after death for forensic diagnosis, because postmortem changes can alter the results [16]. In this tiger, AST (7770 IU/*l*), ALT (5022 IU/*l*), sodium (126 mEq/*l*), potassium (over 10.0 mEq/*l*) and chloride (98 mEq/*l*) could have also been affected by postmortem changes. However, in human forensic pathologic reports, even when postmortem blood was used, BUN values greater than 100 mg/d*l* have been associated with renal disease or acute renal failure due to loss of blood volume, as can occur with hemorrhage [16].

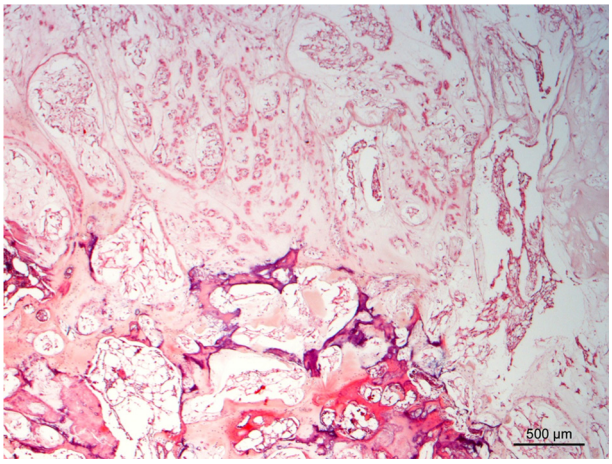

Fig. 3. Microscopic imaging of the mass. The mass was composed of hypocellular myxoid areas, bone and cartilaginous tissues. (H & E. Bar=500 μm). Immunohistochemically, the vacuolated cells were positive for cytokeratin AE1/AE3 and vimentin, but there was no immunoreactivity for S-100 (data not shown). The mass was diagnosed as chordoma based on these findings.

We also considered that severe hypoxia or skeletal muscle damage has been reportedly associated with a high BUN [16]. However, the tiger did not exhibit cyanosis or a low blood oxygen saturation during anesthesia, and there was no history of injury apparent upon physical examination. This tiger was a geriatric (19-year-old) felid, and analysis of urine obtained at almost the same time of starting fluid therapy revealed proteinuria and low urine specific gravity. Furthermore, the necropsy showed moderate chronic nephropathy. These results indicate that the tiger had chronic renal failure. We considered that a decrease in relative blood volume during anesthesia exacerbated the renal dysfunction and that the cause of death was renal failure. Contrast-medium-induced acute kidney injury has been reported in a dog [7] and humans [2], but renal failure connected to contrast medium is unidentified here because it was not possible to conduct extensive preanesthetic evaluation on this tiger.

The CT and MRI characteristics of the chordoma in this tiger were similar to those reported in dogs and humans. It was also considered that combined CT and MRI imaging provides a better technique for the diagnosis of chordoma and metastases than CT or MRI alone. We believe that this report is an important addition to the body of knowledge of imaging characteristics of chordomas in veterinary species.

ACKNOWLEDGMENT. We thank Prof. Kazutaka YAMADA, Obihiro University of Agriculture and Veterinary Medicine for advice regarding the MRI diagnosis.

REFERENCES

1. Carpenter, J. L., Stein, B. S., King, N. W. Jr., Dayal, Y. D. and Moore, F. M. 1990. Chordoma in a cat. *J. Am. Vet. Med. Assoc.* **197**: 240–242. [Medline]

2. Chua, H. R., Horrigan, M., Mcintosh, E. and Bellomo, R. 2014. Extended renal outcomes with use of iodixanol versus iohexol after coronary angiography. *Biomed. Res. Int.* **2014**: 506479. [Medline] [CrossRef]
3. Dunn, D. G., Harris, R. K., Meis, J. M. and Sweet, D. E. 1991. A histomorphologic and immunohistochemical study of chordoma in twenty ferrets (Mustela putorius furo). *Vet. Pathol.* **28**: 467–473. [Medline] [CrossRef]
4. Erdem, E., Angtuaco, E. C., Van Hemert, R., Park, J. S. and Al-Mefty, O. 2003. Comprehensive review of intracranial chordoma. *Radiographics* **23**: 995–1009. [Medline] [CrossRef]
5. Gruber, A., Kneissl, S., Vidoni, B. and Url, A. 2008. Cervical spinal chordoma with chondromatous component in a dog. *Vet. Pathol.* **45**: 650–653. [Medline] [CrossRef]
6. Hadlow, W. J. 1984. Vertebral chordoma in two ranch mink. *Vet. Pathol.* **21**: 533–536. [Medline]
7. Ihle, S. L. and Kostolich, M. 1991. Acute renal failure associated with contrast medium administration in a dog. *J. Am. Vet. Med. Assoc.* **199**: 899–901. [Medline]
8. Kishimoto, R., Omatsu, T., Hasegawa, A., Imai, R., Kandatsu, S. and Kamada, T. 2012. Imaging characteristics of metastatic chordoma. *Jpn. J. Radiol.* **30**: 509–516. [Medline] [CrossRef]
9. Munday, J. S., Brown, C. A. and Weiss, R. 2003. Coccygeal chordoma in a dog. *J. Vet. Diagn. Invest.* **15**: 285–288. [Medline] [CrossRef]
10. Pease, A. P., Berry, C. R., Mott, J. P., Peck, J. N., Mays, M. B. and Hinton, D. 2002. Radiographic, computed tomographic and histopathologic appearance of a presumed spinal chordoma in a dog. *Vet. Radiol. Ultrasound* **43**: 338–342. [Medline] [CrossRef]
11. Seal, U. S., Armstrong, D. L. and Simmons, L. G. 1987. Yohimbine hydrochloride reversal of ketamine hydrochloride and xylazine hydrochloride immobilization of Bengal tigers and effects on hematology and serum chemistries. *J. Wildl. Dis.* **23**: 296–300. [Medline] [CrossRef]
12. Si, M. J., Wang, C. S., Ding, X. Y., Yuan, F., Du, L. J., Lu, Y. and Zhang, W. B. 2013. Differentiation of primary chordoma, giant cell tumor and schwannoma of the sacrum by CT and MRI. *Eur. J. Radiol.* **82**: 2309–2315. [Medline] [CrossRef]
13. Stefanski, S. A., Elwell, M. R., Mitsumori, K., Yoshitomi, K., Dittrich, K. and Giles, H. D. 1988. Chordomas in Fischer 344 rats. *Vet. Pathol.* **25**: 42–47. [Medline] [CrossRef]
14. Stigen, Ø., Ottesen, N., Gamlem, H. and Åkesson, C. P. 2011. Cervical chondroid chordoma in a standard dachshund: a case report. *Acta Vet. Scand.* **53**: 55. [Medline] [CrossRef]
15. Taki, S., Kakuda, K., Kakuma, K., Yamashita, R., Kosugi, M. and Annen, Y. 1996. Posterior mediastinal chordoma: MR imaging findings. *AJR Am. J. Roentgenol.* **166**: 26–27. [Medline] [CrossRef]
16. Uemura, K., Shintani-Ishida, K., Saka, K., Nakajima, M., Ikegaya, H., Kikuchi, Y. and Yoshida, K. 2008. Biochemical blood markers and sampling sites in forensic autopsy. *J. Forensic Leg. Med.* **15**: 312–317. [Medline] [CrossRef]
17. Wippold, F. J. 2nd., Koeller, K. K. and Smirniotopoulos, J. G. 1999. Clinical and imaging features of cervical chordoma. *AJR Am. J. Roentgenol.* **172**: 1423–1426. [Medline] [CrossRef]
18. Woo, G. H., Bak, E. J., Lee, Y. W., Nakayama, H., Sasaki, N. and Doi, K. 2008. Cervical chondroid chordoma in a Shetland sheep dog. *J. Comp. Pathol.* **138**: 218–223. [Medline] [CrossRef]
19. Yan, Z. Y., Yang, B. T., Wang, Z. C., Xian, J. F. and Li, M. 2010. Primary chordoma in the nasal cavity and nasopharynx: CT and MR imaging findings. *AJNR Am. J. Neuroradiol.* **31**: 246–250. [Medline] [CrossRef]